InP nanowire p-type doping via Zinc indiffusion

Haggren, Tuomas; Otnes, Gaute; Mourão, Renato; Dagyte, Vilgaile; Hultin, Olof; Lindelöw, Fredrik; Borgström, Magnus; Samuelson, Lars

Published in:
Journal of Crystal Growth

DOI:
10.1016/j.jcrysgro.2016.06.020

2016

Document Version:
Early version, also known as pre-print

InP Nanowire p-type doping by zinc indiffusion from gas phase

Tuomas Haggren, Gaute Otnes, Renato Mourao, Vilgaile Dagyte, Olof Hultin, Fredrik Lindelöw, Magnus Borgström, Lars Samuelson

http://dx.doi.org/10.1016/j.jcrysgro.2016.06.020

Published in: Journal of Crystal Growth 1 October 2016 451:18-26

InP Nanowire p-type doping by zinc indiffusion from gas phase

Tuomas Haggren, Gaute Otnes, Renato Mourao, Vilgaile Dagyte, Olof Hultin, Fredrik Lindelöw, Magnus Borgström, Lars Samuelson

Abstract

We report an alternative pathway for p-type InP nanowire (NW) doping by indiffusion of Zn species from the gas phase. The indiffusion of Zn was performed in a MOVPE reactor at 350 – 500 °C for 5 – 20 min with either H_2 environment or additional phosphorus in the atmosphere. In addition, Zn_3P_2 shells were studied as protective caps during post-diffusion annealing. This post-diffusion annealing was performed to outdiffuse and activate interstitial Zn. The InP NWs were characterized with photoluminescence and electrical measurements. The acquired carrier concentrations were in order of $>10^{17}$ cm^{-3} for NWs without post-annealing, and up to 10^{18} cm^{-3} for NWs annealed with the Zn_3P_2 shells. The indiffused Zn was evident additionally in the photoluminescence measurements.

Introduction

Semiconductor nanowires (NWs) are promising candidates for numerous applications in future, and most notably so in the field of optoelectronics. To the date, the demonstrated applications include solar cells[1], LEDs[2], transistors[3] and lasers[4]. For these applications, III-V materials are among the most suitable due to their direct band gaps and typically high carrier mobilities. . For InP NWs surface recombination, which can be detrimental to the optical properties, has been reported to be very low[5]. Despite the promising capabilities of InP NWs for solar energy harvesting[1], doping of these NWs poses challenges. Intentional in situ doping has strong effects on the crystal structure and provokes zinc blende (ZB) crystal phase with twinning faults[6]. Such twinning faults could reduce the solar energy harvesting due to charge carrier trapping[7]. Moreover, when growing InP nanowires with the most widely used vapor-liquid-solid technique using Au seed particles as catalysts, p-type doping levels can remain moderate[8]. As a result, creating ohmic contacts to the p-type InP NWs becomes increasingly difficult the lower the doping[9]. An alternative pathway for doping is indiffusion of dopants from gas phase at high temperatures, which has been extensively studied for thin films[9–16], but has been applied to NWs only recently for materials including InAs[17,18], Si[19,20] and ZnO[21]. With diffusion doping, electrical transparency to the NW contacts can be increased significantly via high carrier concentrations near the surface[17,19]. Additionally, site selective doping can be performed, *e.g.* by covering selected parts of the NWs[17,19].

In this work, we apply diffusion doping to InP NWs. The InP NWs were doped p-type by Zn indiffusion in a metalorganic vapor phase epitaxy (MOVPE) reactor, which has showed to provide repeatable diffusion in past research[15]. The highest attained hole concentrations were in the order of 10^{18} cm^{-3}. The optimal conditions for diffusion under H_2 atmosphere and with phosphorus-rich atmosphere are studied. Furthermore, the results show that simpler furnaces suffice for the diffusion process. The indiffusion is examined with electrical and photoluminescence measurements, which are found to be in good

agreement. Moreover, knowledge on Zn indiffusion to NWs is useful regarding unintentional doping when fabricating axial np-junctions.

Experimental and theory

The sample fabrication illustrated in Figure 1. First, the NWs were grown by metalorganic vapor phase epitaxy (MOVPE) in the vapor liquid solid growth mode[22] from Au catalyst particles placed by nanoimprint lithography in a hexagonal array with a pitch of 500 nm. All wires used in the different indiffusion experiments were grown on substrates from the same imprinted wafer, and stems from the same growth run performed in an Aixtron 200/4 growth reactor with a total gas flow of 13 l/min and a working pressure of 100 mbar. A pre-anneal nucleation scheme was used to improve pattern preservation [Otnes, unpublished]. At a growth temperature of 440 °C, growth precursors were TMIn and PH3, at molar fractions of χ_{TMIn}=8.9×10^{-5} and χ_{PH3} = 6.9×10^{-3}, as well as HCl at a molar fraction of χ_{HCl}= 4.6×10^{-5} to suppress radial growth[23]. After the NW growth, the Au seeds were removed by immersing the NWs to H_2SO_4:H_2O (1:10) for 10 s, followed by 10 s immersion to KI:I_2:H_2O (4 g : 1 g : 40 ml), with a DI water rinse in between. This sequence was repeated three times and it removed all of the Au particles. Next, the samples were taken to an Epiquip MOVPE reactor, using a total flow of 6 l/min and a working pressure of 500 mbar, for the diffusion doping process. The diffusion was performed using phosphine (PH_3) and diethylzinc (DEZn), at molar fractions of χ_{PH3} = 6.2×10^{-3} and χ_{DEZn} =5.0×10^{-5}. It is noteworthy here that also sulfur diffusion was attempted with hydrogen sulfide at 500 °C, without any measurable increase in NW conductivity.

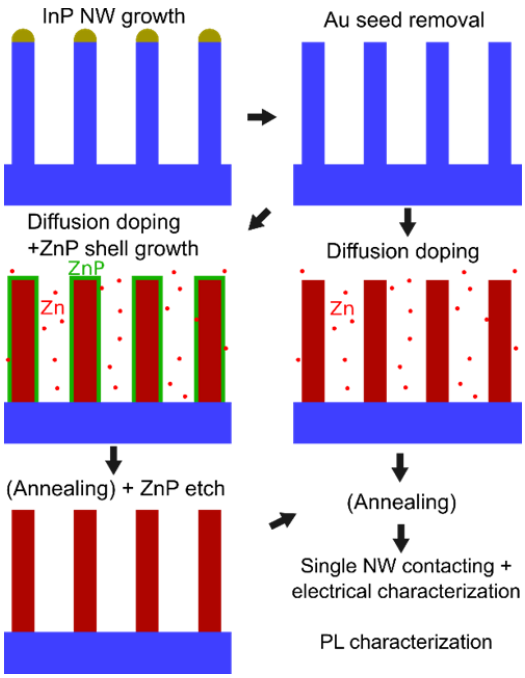

Figure 1. Diffusion doping process for InP NWs. The NWs were grown in a MOVPE reactor, followed by Au seed removal. The NWs were then re-inserted in the MOVPE reactor for Zn diffusion doping and for Zn_3P_2 shell growth for part of the samples. After the diffusion run or after Zn_3P_2 shell removal, some of the samples were annealed in an RTP tool (indicated by "annealing" in brackets). Finally, the NWs were characterized with electrical and photoluminescence measurements. The Zn_3P_2 shells were etched before characterization.

Three different types of diffusion doped NWs were prepared: (i) with H_2 background, (ii) with phosphorus protection by PH_3 flow and (iii) with phosphorus protection and additional Zn_3P_2 shell growth. These different types of diffusion runs are clarified in Figure 2. For the samples without PH_3 in the background, the diffusion at high temperature is expected to damage the NW surface. Therefore, different diffusion temperatures (350 °C, 425 °C and 500 °C) were studied in order to find optimal values for diffusion without considerable damage to the surface. For the other types of samples the background was phosphorus-rich (induced by PH_3 flow). The phosphorus-protected diffusion runs included two types: with and without Zn_3P_2 (ref. 33) shell growth. When the shell growth was avoided, the DEZn flow was turned off after the diffusion step. The third diffusion run type, with Zn_3P_2 shell growth, was otherwise similar except for the open DEZn flow during the cooldown. This prevented the possible Zn outdiffusion during the cooldown and formed Zn_3P_2 shells on the InP cores. Diffusion time effects were studied with the Zn_3P_2 shelled NWs with 5 min, 10 min and 20 min diffusions. For the other samples the diffusion time was 5 min.

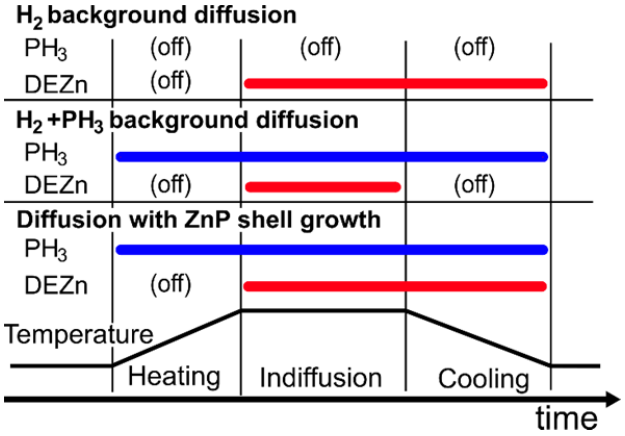

Figure 2. Different processes used for diffusion doping.

After the diffusion step, the NWs were either annealed in a rapid thermal processing (RTP) furnace or taken to electrical and photoluminescence (PL) measurements. The RTP processing was performed at 400 – 500 °C for 5 minutes in order to outdiffuse interstitial Zn, or to activate them to substitutional locations. From the Zn_3P_2 shelled NWs, the shell was removed after the post-diffusion annealing. This etching was done in H_2SO_4:H_2O 1:5 solution. The Zn_3P_2 shells were appeared to be completely removed after 10 s of etching. For the sake of certainty 15 s etch time was used, since no effects were observed on the InP core with this etch time. Only exceedingly long (>60 s) etch steps caused some thinning of the NWs. These and other morphological aspects were studied with scanning electron microscopy (SEM).

Prior to the electrical measurements, the NWs were electrically contacted using electron-beam lithography (EBL). For this purpose, the NWs were transferred to a silicon substrate with 100nm SiO2 and 10 nm HfO2 deposited on top. Subsequently, a polymer lifting layer was deposited in order to avoid the necessity for thick metal contacts. Finally contact patterns were created using EBL and contact metals were evaporated (Pd/Zn/Pd, 5 nm/20 nm/130 nm) and annealed after lift-off for 5 min at 340 °C in N_2. In this study, 6 nanowires were chosen for contacting from each sample. Due to misalignment during EBL exposure and breakages in the evaporated contact metals, contacting was successful for 1-6 of these 6 NWs per sample. The electrical measurements included conventional 4-point current-voltage measurements and back-gate field-effect transistor (FET) type measurements. The back-gate FET

measurement principle and theory using the drude model is explained in detail elsewhere[24]. The carrier concentration *p* can be obtained from the following expression:

$$\sigma = pq\mu, \quad (1)$$

where σ is conductivity, *q* is the elementary charge and μ is the mobility. The mobility is obtained from transconductance g_m with

$$g_m = dI_{SD}/dV_G = C\mu V_{SD}/L^2, \quad (2)$$

where I_{SD} is the source-drain current, V_G is the gate voltage, V_{SD} is the source-drain voltage, *L* is the NW active region length and *C* is the capacitance which is calculated here as follows:

$$C = 2\pi L\varepsilon_0\varepsilon_r / \cosh^{-1}((R+h)/R), \quad (3)$$

where ε_r is the relative dielectric constant, ε_0 is the vacuum permittivity, *R* is the NW radius, and *h* is the distance between the gate and the NW[24]. Several assumptions are made to obtain equation (3), which cause it to give higher capacitance than in reality[24]. In this work, *L* and *R* were acquired from high-magnification SEM images. ε_r value of 3.9 was used for *h* = 102 nm, which was based on the dielectric layers between the gate and the NW (100 nm of SiO_2 and 10 nm of HfO_2). The transconductance was obtained from the back-gate FET measurements by manually fitting a line to the linear region of the measured I_{SD}/V_G curves. The measurements contained also a non-insignificant noise component, which rendered the results only approximately correct. This also contributed to the scattering of the data points. For the V_{SD} values in equation (2), the effective voltage over the active region $V_{SD,eff}$ was calculated with

$$V_{SD,eff} = LI_{SD,max} / \sigma\pi R^2, \quad (4)$$

where $I_{SD,max}$ was the current with maximum V_G. The values obtained for $V_{SD,eff}$ were approximately 10-100 times lower than the used V_{SD} of 1V, indicating considerable voltage drop at the contacts. Therefore, by using $V_{SD,eff}$, the calculated carrier concentrations are 10-100 times lower than by simply using V_{SD} = 1V. It is noteworthy here that since the $1/\sigma$ factor appears in equation (4), it will finally cancel out the σ from equation (1). Therefore, the conductivity obtained from 4-point measurements is decoupled from the carrier concentration measurements and the results can be inspected separately.

Finally, photoluminescence (PL) was measured from NWs that were broken off the growth substrate and transferred to gold patterned silicon substrates. Measurements were performed at low temperature (4K) in a continuous flow liquid helium cooled cold finger cryostat. The NWs were first excited with a frequency doubled yttrium-aluminum garnet (YAG) laser, with excitation wavelength of 532nm after which the luminescence from the nanowire was collected by a microscope objective, dispersed by a grating monochromator and detected by a thermoelectrically cooled CCD camera.

Results and discussion

Microscopy and electrical characterization

In order to study the optimal diffusion temperature and feasibility of the diffusion doping to basic oven type tools, the Zn diffusion was attempted under H_2 atmosphere at 350 – 500 °C. SEM images of the NWs before the diffusion run and afterwards are shown in Figure 3. Annealing without phosphorus in

the atmosphere has been shown to deteriorate or decompose InP surface already at 250 – 300 °C, mainly via phosphorus evaporation[25–27]. Therefore, a diffusion run was performed at 500 °C also with phosphorus-rich atmosphere, i.e. with PH_3 flow on. The SEM images (Figs. 3b-d) show that the diffusion under H_2 had two visible effects on the NWs: surface roughness and nano-sized islands that formed on NW sidewalls and tips. In a study on InP substrate annealing without phosphorus protection, In droplets formed due to loss of phosphorus from the substrate[28]. The islands on the NW sidewalls are likely created in a similar way, however, due to the Zn-rich environment the islands might contain Zn in addition to In in our case. The islands tended to detach during contact processing and small holes were observed instead (Fig. 3f), indicating that the islands formed in etch pits as suggested in earlier work[28]. The diffusion under P-rich atmosphere, on the other hand, had no observable effect on the NWs (Fig. 3e). On the contrary, these NWs appeared identical in SEM before and after the diffusion run.

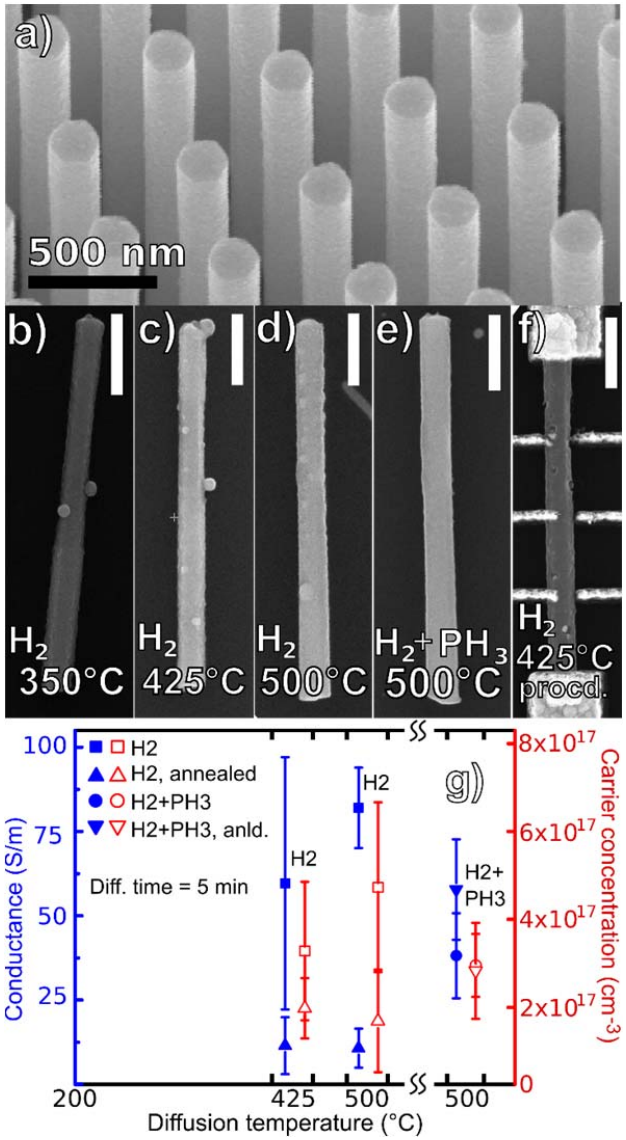

Figure 3. SEM images of an InP NW array after Au seed removal (a), NWs diffused under H_2 background (b-d), NW diffused with H_2 + PH_3 background (e), and NW diffused under H_2 after processing (f). All scale bars correspond to 500nm. Conductivity and carrier concentration data from these NWs is presented in (g) with the background and annealing indicated in the label.

The diffusion temperature effects on carrier concentration and conductivity are shown in Figure 3g. The 350 °C diffusion resulted in values that were too small to interpret and is therefore omitted from the graph. It is noteworthy here that non-intentionally doped NWs showed open channel with positive gate voltage (that accumulates electrons) in the back-gate FET measurements. This indicates that the non-intentionally doped NWs were slightly n-type, which is characteristic for MOVPE-grown InP NWs[8]. Therefore, the original n-type doping has to be compensated prior to obtaining the p-type behavior, which in part explains the poor conductivity of the NWs diffused at 350 °C. When the diffusion temperature was 425 °C, the carrier concentration and the conductivity increased notably, giving the measured values presented in Figure 3g. Further increase in the diffusion temperature to 500 °C gave additional ~50 % increase in carrier concentration and conductivity compared to the 425 °C diffused sample. This corresponds well to the literature, where optimal temperatures have been reported around 500 °C [10,29,30]. The optimal temperature range results from zinc phosphide growth at lower temperatures and evaporation of Zn species at higher temperatures[29,30].

Post-annealing is an essential part of the diffusion doping process, since a considerable part of the diffused Zn take interstitial positions (Zn_i), where they can act as donors and compensate the p-type doping[10,12,16,28,30]. Additionally, hydrogen can effectively passivate Zn acceptors[31]. The post-annealing process activates the interstitial Zn_i to substitutional positions (Zn_s), and outdiffuses mainly the Zn_i and hydrogen[16,28,30]. In addition, a slow loss of Zn_s is indicated by a reduced carrier concentration after prolonged (8 h) annealing in earlier work[16]. While the outdiffusion and activation of Zn_i (increasing hole concentration) is competing with the outdiffusion of Zn_s (reducing hole concentration), the latter is a much slower process and therefore typically negligible. In NWs, however, the effect is pronounced due to the high surface-to-volume ratio. In the earlier research with planar structures, the topmost few hundred nm show reduced carrier concentration compared to deep regions of the crystal[10,15,16]. Therefore, outdiffusion of substitutional Zn might not be negligible with NWs and should be taken into consideration when dealing with diffusion doped NWs.

We now turn our focus to post-annealed NWs, i.e. NWs annealed after indiffusion *ex-situ* under N_2 atmosphere at 400 °C in an RTP tool. Figure 3g shows that for the NWs diffused with PH_3 protection, the annealing caused little difference in carrier concentration or in conductivity. This can be due to the small number of donor-type Zn_i after 5 minutes of diffusion, which is supported by findings from core-shell NWs as will be explained later in this paper. Alternatively, the competing processes could be of the same magnitude for these NWs. On the other hand, when the NWs were diffused without P protection under H_2, the post-annealing process reduced the carrier concentration and the conductivity. Since the most distinct difference between these NWs is the surface properties, it likely causes the reduction as well, possibly via the introduction of additional trap-like surface states during the post-diffusion annealing step. These in turn could increase the band bending (which is typical for p-InP NWs[32]) and diminish the conductive channel. Since the calculations assumed the channel width to equal the NW diameter, the diminished conductive channel would make the conductivity and carrier concentration values appear smaller. This is in accord with the observed results shown in Fig. 3g, and it is likely that the measured

values only appear smaller after annealing, while the reduction is in fact due to the reduced conductive channel. As for the morphological effects observed in SEM after the annealing, the sample diffused with P protection showed no observable changes, while the nanoislands appeared melted on the sidewalls of the NWs diffused under H_2.

The acquired carrier concentrations in the order of 10^{17} cm^{-3} are useful for applications where high carrier concentrations are not necessary. As such, diffusion provides an alternative pathway for p-type nanowire doping, which can be performed *ex-situ* with any furnace in which Zn species can be introduced under controlled gas flows. This offers new possibilities for planning different structures, since the diffusion takes place only on the areas exposed to the gases. However, numerous envisioned device structures require ohmic contacts for which doping levels of 10^{18} – 10^{19} cm^{-3} are desirable[9]. To strive for this, another processing scheme was developed, where the outdiffusion is mitigated with a core-shell structure. By mitigating outdiffusion the activation of interstitial Zn is enhanced as well, since the slower rate of outdiffusion increases the probability of activation. The shell used in this study was Zn_3P_2, which is typically grown at 300 –450 °C in MOVPE[33]. Zn_3P_2 itself is a direct ~1.5 eV band-gap semiconductor that has recently attracted attention for heterojunction solar cells[34]. Additionally, it has contributed to ohmic contact creation to p-InP[35]. It is noteworthy here that in earlier work the approach of coating diffusion doped InP layers with SiN cap prior to post-annealing has not increased the carrier concentration[16]. This is in contrast to our results, which could be due to the coating material that was Zn_3P_2 in our work, especially since Zn_3P_2 has been used as a source material for diffusion doping[16].

Figure 4 shows SEM images of the NWs diffused with the Zn_3P_2 shell growth process and electrical measurement data collected from these NWs after removal of the shell. The NWs with Zn_3P_2 shells appear hexagonal, indicating epitaxial growth (Fig. 4a). However, the rough sidewalls point to a polycrystalline structure. The shells were etched in order to reveal and measure the InP NW cores. The etching was observed to cause little effects on the InP NW, i.e. shallow lines perpendicular to the growth direction appeared on the InP surface (e.g. Fig. 4c-d,f). When the Zn_3P_2-shelled NWs were annealed at 400 °C, the appearance in SEM remained the same as before the annealing for both Zn_3P_2-shells (Fig. 4b) and the InP cores after the shell removal (Fig. 4c-d). However, after annealing at 500 °C, the InP cores exhibited serious surface damage (Fig. 4e), indicating that the InP core reacted with the Zn_3P_2 shell. Therefore, 400 °C was a more suitable temperature for the annealing.

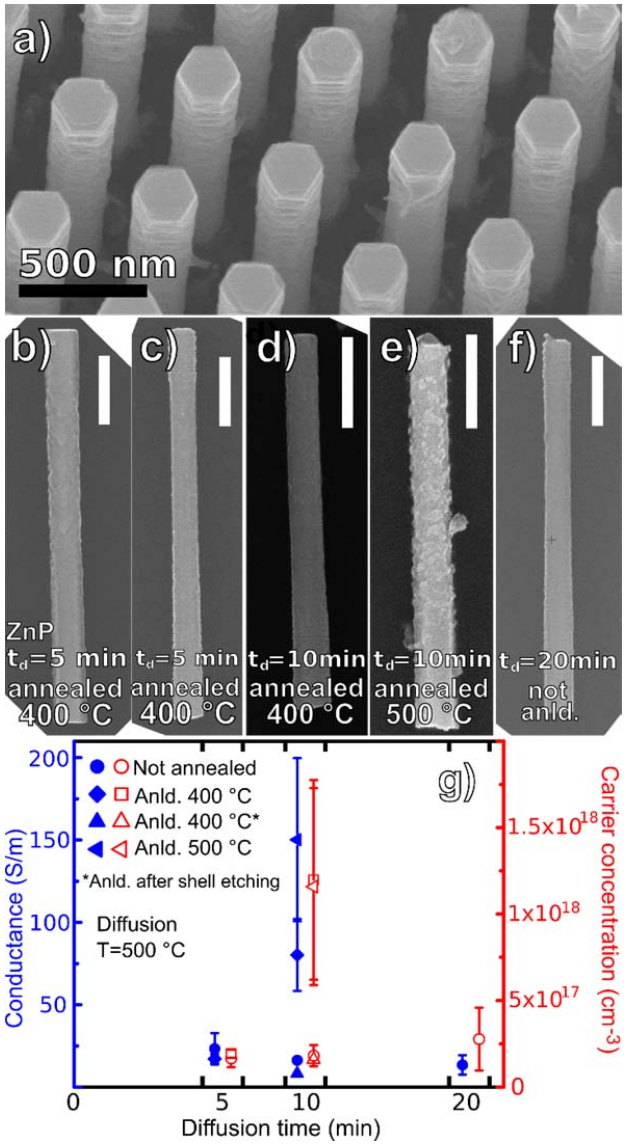

Figure 4. SEM images of an InP NW array after Zn indiffusion and Zn_3P_2 shell growth (a), 5 min diffused, Zn_3P_2 shelled NW after annealing at 400 °C before (b) and after (c) shell removal, 10 min diffused NW after annealing at 400 °C (d) and 500 °C (e) (shells removed), and 20 min diffused NW after the shell removal (f). All scale bars correspond to 500nm. Conductivity and carrier concentration data from the NWs diffused with Zn_3P_2 shell growth process is presented in (g).

When the electrical measurements were performed on these NWs after the shell removal (without post-annealing with the shell), the carrier concentrations were on the same order of magnitude, 10^{17} cm^{-3}, as the NWs diffused without the Zn_3P_2 shell growth (Figures 3g and 4g). This indicates that the shell growth and removal as such had little effect on the electrical properties of the NWs. Additionally, the diffusion time had no major effect on the non-annealed NWs, which is seen as only slight increase in carrier concentration and in conductivity when the diffusion time was increased from 5 min to 20 min. This can be explained either by saturated diffusion already at 5 min, or by even distribution to acceptor and donor type sites of the additional Zn after 5 min. Of these explanations, the latter one is supported by

the measurements on the NWs which were annealed at 400 – 500 °C after the growth and prior to shell removal. Figure 4g shows that the carrier concentration and the conductivity barely increased for the 5 min diffused sample, whereas the 10 min diffused sample shows considerable increase up to 10^{18} cm^{-3} or >100 S/m. Considering that the 10 min diffused sample showed no enhancement if the annealing was performed *after* the shell removal (see Fig. 4g), it is clear that the Zn_3P_2 shell was essential during the annealing in obtaining the increased carrier concentration and conductivity. On the other hand, the indiffusion during the first 5 minutes results mainly in substitutional acceptor-type dopants, since the post-annealing did not improve the carrier concentration with the 5 minutes diffused sample. Group III vacancies have efficiently captured diffusing Zn in past research[13], and in our work these vacancies appear to saturate during the first 5 minutes of diffusion. The subsequent diffusion then increases the interstitial and substitutional Zn nearly evenly, which is seen as a rather stagnant carrier concentration with increased diffusion time, unless the post-annealing is performed with the Zn_3P_2 shells.

Photoluminescence characterization

In addition to the electrical measurements, the NWs were characterized with photoluminescence. The as-grown nanowires show 4K PL peaks at about 1.42eV and 1.47eV, which correspond to ZB and WZ phases, respectively (Fig. 5). In addition, several weaker peaks emerged around these main peaks, and they are attributed to type II transitions between ZB and WZ phases, and to quantisized energies due to alternating phases. On the other hand, NWs with Zn diffusion showed significantly redshifted signal, while the tendency remained to exhibit one or two separate strong peaks accompanied by weaker and shoulder peaks. Examples of PL graphs of Zn diffused NWs are presented in Figure 5.

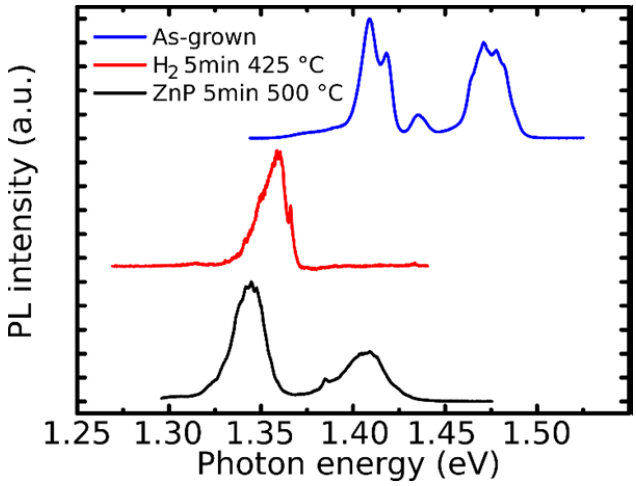

Figure 5: Typical PL spectra from an as-grown and diffusion doped InP nanowires (5min diffusion under H_2 background and with Zn_3P_2 shell growth process, after shell removal).

PL data from a larger sampling is presented in Figure 6a, i.e. PL peak positions measured from 5-6 individual nanowires from as-grown NWs (marked with 0 min diffusion) and from NWs diffused at 500 °C for 5 – 20 min. For these NWs, the diffusion was performed with PH_3 protection and included the Zn_3P_2 shell growth. After the diffusion and shell removal, the peak positions had redshifted by 50 – 80

meV. Two different groups of strong peaks remain after the diffusion, one in the region 1.33 – 1.36 eV and the other close to 1.41 eV. The value of the higher energy group is close to ZB InP band-to-band transition. However, since this peak was present even in the most heavily diffused samples, it is more likely related to indiffused Zn. Moreover, band-to-band transitions have been absent in previous PL studies on Zn diffused InP[12,36]. Therefore, a more plausible origin for the 1.41 eV peak is WZ segments that exhibit redshifted signal (likewise to the 1.36 eV peaks that results from redshifted transition in ZB segments).

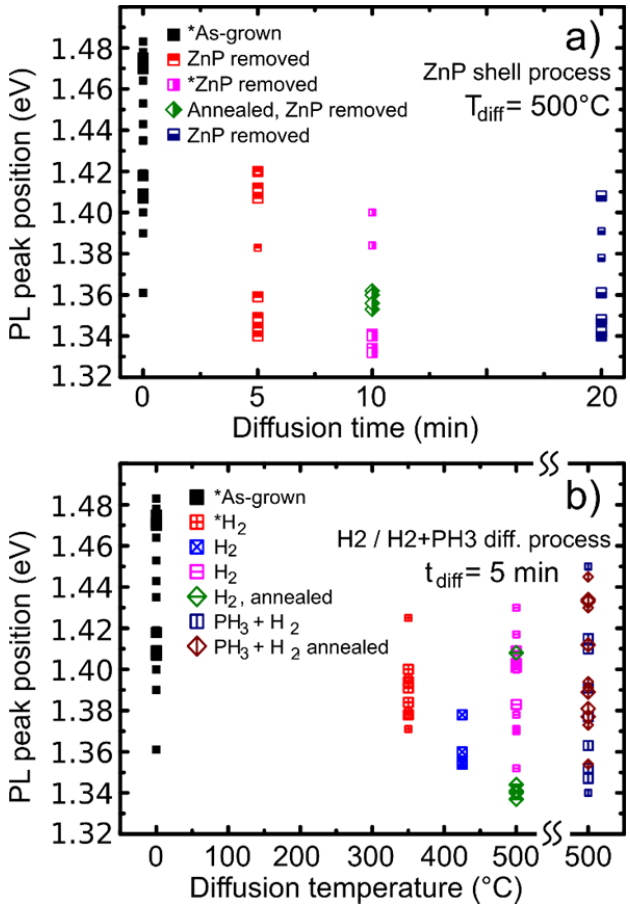

Figure 6. PL peak positions from NWs diffused with Zn_3P_2 shell growth process at 500 °C for 5 – 20 min and from a reference sample (a), and from NWs diffused at 350 – 500 °C for 5 min under H_2 atmosphere with or without PH_3 protection (b). The reference samples are marked as 0 min or 0 °C diffusion. The large symbols show the positions of the main peaks, and the small symbols show weak and shoulder peaks. Annealed samples are marked with tilted squares. Asterisk in the label indicates 10 % of maximum laser intensity instead of 3 %.

Regarding the origin of the redshift, PL peaks have been between 1.3 and 1.38 eV in earlier studies on Zn diffused InP[12,36]. In both of these studies the transitions with low-end energies were attributed to donor-acceptor pairs, where substitutional Zn_s acts as an acceptor, and interstitial Zn_i acts as a donor. The donor-type behavior of Zn_i is supported in several other reports[10,11,16], and it results in significantly higher Zn atomic concentration (C_{tot}) compared to Zn_s concentration (C_s). In the earlier studies, the high-end PL peak energies were obtained when interstitial donor concentration (C_i) was reduced via

annealing, up to the highest value of 1.38 eV when C_{tot} equals to C_s (ref. 12,36). Comparing the PL peak positions from non-annealed NWs in Figure 6a to these earlier reports, the values correspond to partially outdiffused or activated Zn_i, i.e. when $C_s > C_i \neq 0$. On the other hand, p-type InP NWs that were doped during the growth have also showed redshifted signal due to Fermi level pinning and resulting band bending[32]. Therefore, in the case of diffusion doped p-InP NWs, both transitions related to Zn_i and Zn_s, and the band bending effects are likely to contribute to the redshift.

It is noteworthy here that the interstitial Zn can take different locations within the InP crystal, which correspond to various energy positions in the InP band gap[12]. As a result, also the PL peak position varies according to the interstitial lattice site. The local variation of the peak position observed here is also attributed to these different interstitial sites.

Effects of post-annealing on PL were studied with the sample diffused for 10 min with the Zn_3P_2 shell growth process. This sample was characterized after post-annealing at 400 °C and subsequent shell removal. The annealing resulted in a blueshift of approximately 20 meV, which indicates increased C_s/C_i ratio. Since the back-gate FET measurements showed significantly increased carrier concentration as well, these measurements are in a good agreement.

In addition to the diffusion time, the diffusion temperature effects on PL were studied. Figure 6b shows PL peak positions from samples diffused at 350 - 500 °C under H_2 atmosphere, along with an as-grown reference sample (marked with 0 °C diffusion). The signal redshifted already with samples diffused at 350 °C. This suggests that Zn diffusion took place already at 350 °C, while it remained exceedingly low to measurable in the electrical characterization. Additionally, the redshift is smaller than for samples diffused at 425 °C or at 500 °C (Figure 6b). The lesser redshift also suggests that the indiffusion was weaker. The band bending in p-InP NWs occurs due to holes being trapped at donorlike surface states[32], and a low amount of available holes induces weaker band bending and thus weaker redshift.

Diffusion at 425 °C resulted in a redshift comparable to those at 500 °C with Zn_3P_2 shell growth, suggesting that this temperature was adequately high for Zn indiffusion. This was seen also in the electrical measurements as the carrier concentration was comparable to the samples diffused at 500 °C. When the diffusion temperature is raised to 500 °C without PH_3 protection, the PL signal intensity decreased significantly (not shown here), and the peak positions were scattered and less redshifted. As discussed earlier, the diffusion process without phosphorus protection is expected to damage the NW surface, and this damage is more severe at higher temperatures. The results indicate that diffusion at 500 °C without phosphorus is detrimental to the surface, and the optimal temperature for this process is around 425 °C.

From the samples diffused at 500 °C, the NWs diffused with PH_3 protection were measured in addition to the NWs discussed above (without PH_3 protection). The PL spectra from these NWs contained one or two clear peaks with few or no weak peaks and shoulder peaks. The peaks were rather scattered between ~1.35 eV and 1.42 eV, while all spectra showed a non-insignificant emission around 1.35 eV. In these NWs, partial outdiffusion of Zn_i might occur during the DEZn-free cooldown. Considering the electrical measurement results, the outdiffusion would not be expected, but it is assumed here that already small changes in C_i can affect the redshift. This is supported by the redshifted PL signal from the sample diffused at 350 °C, from which the electrical measurements showed no improvement, and for which the amount of indiffused Zn was deemed low. The scattered peak positions suggest varying degree of outdiffusion, as it depends on the C_s/C_i ratio. However, when these NWs were annealed at

500 °C after the diffusion run, the peaks remained scattered through the same energy range, and the only notable effect was broadening of the peaks (which probably results from surface damage during the post-annealing). This suggests that the outdiffusion during the post-annealing did not affect the C_s/C_i ratio significantly. In other words, this also indicates that only little Zn_i was present after 5 minutes of diffusion, as was assumed earlier.

Finally, power dependency measurements are shown in Figure 7. The peaks were separated in two groups, namely around 1.36 eV and around 1.42 eV at full intensity. For the NWs without post-annealing (Fig. 7a), both of these groups blueshifted at similar rates towards higher intensity. For most of the measured samples, the blueshifting occurs even at very low excitation intensities. There are two likely contributors to the blueshift, (i) state filling and (ii) reduced band bending [32]. The state filling (i) results in the lowest-energy transitions being no longer available. These lowest-energy transitions could originate from certain interstitial states that are filled when the number of charge carriers increases. Zn atoms can occupy different interstitial locations that give rise to different donor states in the band gap[12], and these states can then become filled as the intensity increases. The other contributor, band bending related blueshift (ii), is explained in detail elsewhere[32]. In short, the larger number of generated charge carriers diminishes the band bending, thereby raising the electrons near the surface to higher energies relative to the valence band maximum where the holes reside.

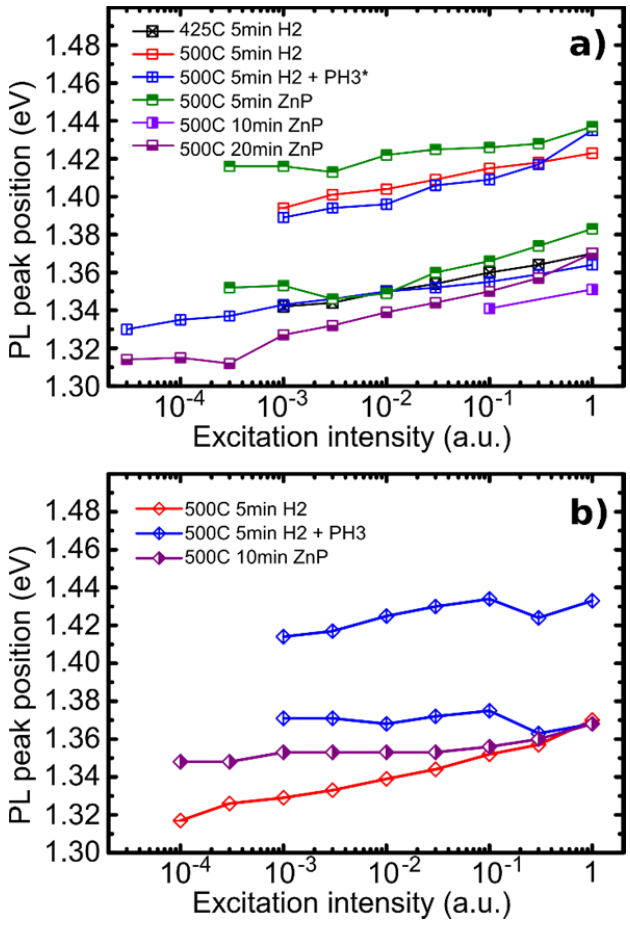

Figure 7: Power dependency measurements of PL peak positions (a) from as-diffused InP NWs and after Zn_3P_2 shell removal, and (b) from NWs after post-annealing at 400 °C. Asterisk in the label in (a) denotes signal from 2 separate NWs. The connecting lines serve as a guide for the eye.

Figure 7b shows PL peak power dependencies measured after the post-diffusion annealing step. From these, the two samples diffused with phosphorus protection showed clearly smaller dependence on the excitation intensity after the annealing. For these samples, the electrical measurements showed increased or similar hole concentration after the post-annealing step, which should result in similar or increased band bending, and the effect on PL shifting should be the same. Since the shifting of the PL peaks decreased, the band bending appears to have minor significance for these samples, and instead the changes in the power dependency are dominated by the state filling phenomenon. In other words, the lesser dependence on the excitation power suggests that the lowest-energy states no longer exist. This is in accord with the expected results from the post-annealing, *i.e.* reduced number of Zn_i. The interstitial positions that gave rise to the lowest-energy transitions could have transformed to either substitutional positions or outdiffused altogether.

A different behavior after annealing is observed for the sample diffused without phosphorus protection. For this sample, the magnitude of the power dependency remained unchanged. As discussed earlier, the diffusion without phosphorus protection appeared to deteriorate the surface which could also increase the density of the surface states. Therefore, the band bending is stronger and has a clear effect on the PL also after the post-annealing step, which is in accord with the observations discussed earlier from the electrical measurements.

Conclusions

In conclusion, we report p-type doping of InP NWs by Zn indiffusion. The studied diffusion characteristics included carrier concentration, conductivity and photoluminescence, and all of these were found to be in a good agreement. The diffusion takes place at as low temperatures as 350 °C (based on redshifted PL signal), while considerable carrier concentration (>10^{17} cm^{-3}) was acquired from NWs diffused at 425 – 500 °C. However, diffusion at 500 °C without phosphorus protection was detrimental to the NW surface, which was seen as reduced PL signal intensity and in SEM. Therefore, approximately 425 °C is the most suitable temperature for Zn indiffusion without phosphorus protection. When the diffusion at 500 °C was performed with PH_3 in the background, the surface damage was avoided. Considerably higher carrier concentration up to 10^{18} cm^{-3} was obtained when the NWs were coated with a Zn_3P_2 shell and annealed at 400 – 500 °C after the diffusion. The increased carrier concentration required also 10 min diffusion time, and shorter (5 min) diffusion time being insufficient was attributed to Zn occupation mostly in substitutional locations during the first 5 minutes, and to prevailing interstitial locations thereafter. These interstitials can then be activated in the post-annealing step. The annealing step was not beneficial for the NWs without Zn_3P_2 shells, possibly due to competing outdiffusion of substitutional, acceptor-type Zn. The presented results offer an alternative pathway for InP NW doping, with the possibility for selective doping by covering parts of the NWs, which can be useful for various device structures. Furthermore, relatively simple furnaces suffice for the diffusion doping.

Acknowledgements

The authors acknowledge Alexander Berg for fruitful discussions and for the aid with the Au particle removal. T. Haggren wishes to thank Emil Aaltonen Foundation, Ulla Tuominen Foundation and Walter

Ahlström Foundation for supporting the research. This work was performed within the Nanometer Structure Consortium at Lund University (nmC@LU) and supported by the Swedish Research Council (Vetenskapsrådet), by the Swedish Energy Agency, and by the EU programme PhD4Energy under Grant 608153. This project has received funding from the *European Union's Horizon 2020 research and innovation programme* under grant agreement No 641023.

(1) Wallentin, J.; Anttu, N.; Asoli, D.; Huffman, M.; Aberg, I.; Magnusson, M. H.; Siefer, G.; Fuss-Kailuweit, P.; Dimroth, F.; Witzigmann, B.; Xu, H. Q.; Samuelson, L.; Deppert, K.; Borgström, M. T. *Science* **2013**, *339* (6123), 1057–1060.

(2) Qian, F.; Gradečak, S.; Li, Y.; Wen, C.-Y.; Lieber, C. M. *Nano Lett.* **2005**, *5* (11), 2287–2291.

(3) Goldberger, J.; Hochbaum, A. I.; Fan, R.; Yang, P. *Nano Lett.* **2006**, *6* (5), 973–977.

(4) Huang, M. H.; Mao, S.; Feick, H.; Yan, H.; Wu, Y.; Kind, H.; Weber, E.; Russo, R.; Yang, P. *Science* **2001**, *292* (5523), 1897–1899.

(5) Joyce, H. J.; Wong-Leung, J.; Yong, C.-K.; Docherty, C. J.; Paiman, S.; Gao, Q.; Tan, H. H.; Jagadish, C.; Lloyd-Hughes, J.; Herz, L. M.; Johnston, M. B. *Nano Lett.* **2012**, *12* (10), 5325–5330.

(6) Algra, R. E.; Verheijen, M. A.; Borgström, M. T.; Feiner, L.-F.; Immink, G.; van Enckevort, W. J. P.; Vlieg, E.; Bakkers, E. P. A. M. *Nature* **2008**, *456* (7220), 369–372.

(7) Wallentin, J.; Ek, M.; Wallenberg, L. R.; Samuelson, L.; Borgström, M. T. *Nano Lett.* **2012**, *12* (1), 151–155.

(8) Borgström, M. T.; Norberg, E.; Wickert, P.; Nilsson, H. A.; Trägårdh, J.; Dick, K. A.; Statkute, G.; Ramvall, P.; Deppert, K.; Samuelson, L. *Nanotechnology* **2008**, *19* (44), 445602.

(9) Vanhollebeke, K.; D'Hondt, M.; Moerman, I.; Van Daele, P.; Demeester, P. *J. Cryst. Growth* **2001**, *233* (1-2), 132–140.

(10) Wada, M.; Sakakibara, K.; Higuchi, M.; Sekiguchi, Y. *J. Cryst. Growth* **1991**, *114* (3), 321–326.

(11) Schade, U.; Enders, P. *Semicond. Sci. Technol.* **1992**, *7* (6), 752–757.

(12) Montie, E. A.; van Gurp, G. J. *J. Appl. Phys.* **1989**, *66* (11), 5549.

(13) König, U.; Haspeklo, H.; Marschall, P.; Kuisl, M. *J. Appl. Phys.* **1989**, *65* (2), 548.

(14) Kazmierski, K.; Huber, A. M.; Morillot, G.; Cremoux, B. de. *Jpn. J. Appl. Phys.* **1984**, *23* (Part 1, No. 5), 628–633.

(15) Hampel, C. A.; Blaauw, C.; Calder, I. D.; Glew, R.; Macquistan, D.; Bryskiewicz, T.; Guillon, S. *J. Vac. Sci. Technol. A Vacuum, Surfaces, Film.* **2004**, *22* (3), 912.

(16) van Gurp, G. J.; van Dongen, T.; Fontijn, G. M.; Jacobs, J. M.; Tjaden, D. L. A. *J. Appl. Phys.* **1989**, *65* (2), 553.

(17) Ho, J. C.; Ford, A. C.; Chueh, Y.-L.; Leu, P. W.; Ergen, O.; Takei, K.; Smith, G.; Majhi, P.; Bennett, J.; Javey, A. *Appl. Phys. Lett.* **2009**, *95* (7), 072108.

(18) Ford, A. C.; Chuang, S.; Ho, J. C.; Chueh, Y.-L.; Fan, Z.; Javey, A. *Nano Lett.* **2010**, *10* (2), 509–513.

(19) Moselund, K. E.; Ghoneim, H.; Schmid, H.; Björk, M. T.; Lörtscher, E.; Karg, S.; Signorello, G.; Webb, D.; Tschudy, M.; Beyeler, R.; Riel, H. *Nanotechnology* **2010**, *21* (43), 435202.

(20) Garnett, E. C.; Tseng, Y.-C.; Khanal, D. R.; Wu, J.; Bokor, J.; Yang, P. *Nat. Nanotechnol.* **2009**, *4* (5), 311–314.

(21) Chang, L.-T.; Wang, C.-Y.; Tang, J.; Nie, T.; Jiang, W.; Chu, C.-P.; Arafin, S.; He, L.; Afsal, M.; Chen, L.-J.; Wang, K. L. *Nano Lett.* **2014**, *14* (4), 1823–1829.

(22) Wagner, R. S.; Ellis, W. C. *Appl. Phys. Lett.* **1964**, *4* (5), 89.

(23) Borgström, M. T.; Wallentin, J.; Trägårdh, J.; Ramvall, P.; Ek, M.; Wallenberg, L. R.; Samuelson, L.; Deppert, K. *Nano Res.* **2010**, *3* (4), 264–270.

(24) Wallentin, J.; Borgström, M. T. *J. Mater. Res.* **2011**, *26* (17), 2142–2156.

(25) Iyer, R. *J. Vac. Sci. Technol. B Microelectron. Nanom. Struct.* **1988**, *6* (4), 1174.

(26) Farrow, R. F. C. *J. Phys. D. Appl. Phys.* **1974**, *7* (17), 2436–2448.

(27) Tseng, W. *J. Vac. Sci. Technol.* **1981**, *19* (3), 623.

(28) Wong, C.-C. D.; Bube, R. H. *J. Appl. Phys.* **1984**, *55* (10), 3804.

(29) van Geelen, A.; de Smet, T. M. F.; van Dongen, T.; van Gils, W. M. E. M. *J. Cryst. Growth* **1998**, *195* (1-4), 79–84.

(30) Wisser, J.; Glade, M.; Schmidt, H. J.; Heime, K. *J. Appl. Phys.* **1992**, *71* (7), 3234.

(31) Dautremont-Smith, W. C.; Lopata, J.; Pearton, S. J.; Koszi, L. A.; Stavola, M.; Swaminathan, V. *J. Appl. Phys.* **1989**, *66* (5), 1993.

(32) van Weert, M. H. M.; Wunnicke, O.; Roest, A. L.; Eijkemans, T. J.; Yu Silov, A.; Haverkort, J. E. M.; 't Hooft, G. W.; Bakkers, E. P. A. M. *Appl. Phys. Lett.* **2006**, *88* (4), 043109.

(33) Suda, T.; Kakishita, K. *J. Appl. Phys.* **1992**, *71* (6), 3039.

(34) Bosco, J. P.; Demers, S. B.; Kimball, G. M.; Lewis, N. S.; Atwater, H. A. *J. Appl. Phys.* **2012**, *112* (9), 093703.

(35) Park, M.-H.; Wang, L. C.; Cheng, J. Y.; Deng, F.; Lau, S. S.; Palmstrøm, C. J. *Appl. Phys. Lett.* **1996**, *68* (7), 952.

(36) Hsu, J. K. *J. Vac. Sci. Technol. B Microelectron. Nanom. Struct.* **1994**, *12* (3), 1416.